



Synthesis and Application of Electrospun Nickel-Molybdenum/Graphene Composite Nanofibers and Nickel-Molybdenum Nanofibers Supported on Graphene Nanosheets Catalysts for Hydrocracking of Heavy Hydrocarbons

Behzad Zanjanejad , Amirfarhad Noroozi Moghaddam , Mokhtar A. Babatabar , Ahmad Tavasoli*

1. University of Tehran, Tehran, Iran. E-mail: behzadzanjanejad4@gmail.com
2. University of Tehran, Tehran, Iran. E-mail: amirfarhad.norozi@ut.ac.ir
3. University of Tehran, Tehran, Iran. E-mail: m.babatabar@ut.ac.ir
4. University of Tehran, Tehran, Iran. E-mail: tavasoli.a@ut.ac.ir

ARTICLE INFO	ABSTRACT
<p>Article History: Received: 11 September 2024 Revised: 06 March 2025 Accepted: 10 March 2025 Published: 10 March 2025</p> <p>Article type: Research</p> <p>Keywords: Coke, Graphene, Hydrocracking, Molybdenum, Nanofibers, Nickel</p>	<p>Electrospun NiMo/Graphene composite nanofibers (NMGF) and NiMo nanofibers supported on Graphene nanosheets (NMFG) were prepared via the electrospinning technique. Their performance for the hydrocracking of n-hexadecane (n-C₁₆) was compared with the NiMo/Graphene (NMG) synthesized by the conventional impregnation method and commercial NiMo/γ-Al₂O₃ (NMA) catalysts in a fixed-bed reactor. ICP, BET, TEM, FESEM, XRD, and NH₃-TPD tests were used to characterize the produced catalysts. The performance of the catalysts was evaluated based on total conversion and the distribution of liquid products over a continuous reaction period of 120 hours. The uniform dispersion of fibers, high surface area, large pore volume, and stronger acidic sites of NMGF and NMFG catalysts resulted in high percentage conversions of 99.5 and 99.2, respectively. The lighter hydrocarbons were achieved in hydrocracking using nanofibrous catalysts. Furthermore, nanofibrous catalysts produced a more stable catalyst than their counterparts, which suffered from coke production and deactivation of roughly 6% over 120 hours. The obtained results revealed the high potential of fibrous catalysts synthesized via the electrospinning method compared with conventional metal oxide nanoparticles-supported catalysts for hydrocracking heavy oils.</p>

Introduction

The conversion of heavy crude oil to valuable middle distillates has recently been of interest to industrial groups [1-12]. Among various methods, including gasification, solvent extraction, viscosity reduction, coking, and hydrocracking (HC), the HC is the most suitable method for the simultaneous conversion of heavy oils and vacuum residues into middle distillates and removal of impurities such as sulfur, nitrogen, and metals [12-20]. The reactor system and catalyst properties play significant roles in the hydrocracking yield of heavy oils. Among various reactor systems, including moving-bed, ebullated-bed, and fixed-bed reactors (FBRs), the FBR system, due to the simplicity of operation and easier scale-up, is the most efficient reactor system for upgrading heavy oils and residues [21-33]. However, the main challenge of the fixed-bed hydrocracking reactor is the gradual decline in catalyst activity [7]. Thus,

*Corresponding Author: A. Tavasoli (E-mail address: tavasoli.a@ut.ac.ir)



improving the catalyst lifetime and activity for increasing the middle distillate products from the cracking of long-chain paraffins is the main challenge [26, 27]. The metallic sites' properties, the physicochemical properties of the support, such as pore diameter, acidity, and their balance in the bifunctional catalyst, should be considered for decreasing the diffusion limitations and optimizing the catalyst activity toward hydrocracking of heavy oils [11, 14, 30].

Various supports, including zeolites [17, 20], metal-organic frameworks [16], activated carbon [25], carbon nanotubes [5, 22, 28, 29], and graphene [12, 31, 34, 35], have been used for the synthesis of supported metal catalysts. Graphene nanosheets (GNS) have been utilized as catalyst support in various catalytic applications due to their exceptional physicochemical stability and extensive surface area [12, 35]. Furthermore, in recent studies, the activity of nanocatalysts was increased by converting nanomaterials to the fibrous form via the electrospinning process [1]. The electrospun nanofibrous catalysts showed significant activity for the hydrocracking of heavy oils because of their large surface area, low agglomeration, and ease of recovery [2]. The high surface area and low aggregation cause the high contents of active sites per mass of materials during the hydrocracking of heavy oils [1, 36]. Recently, zeolite nanofibers have been used to support the cracking process efficiently. Anis et al. synthesized the nickel oxide-tungsten oxide/zeolite nanofibers via the electrospinning method for n-heptane hydrocracking [1]. The results indicated low coke formation with high conversion efficiency using nanofibers compared with the performance of the catalyst synthesized by the wet impregnation method. Anis et al. also investigate the potential of NiO-WO₃ over the Y-zeolite nanofibrous support for hydrocracking of n-heptane [2]. Kaminski et al. [8] investigated the hydrocracking of Athabasca vacuum residue using fibers composed of zeolite Y-NiO-WO₃ as the catalyst. Puron et al. [21] compared the potential of NiMo catalyst over the alumina and carbon nanofibers supports for hydrocracking a vacuum residue. Although relatively larger amounts of lighter products were obtained in the presence of the Al₂O₃-supported catalyst, the coke formation was very low using carbon nanofiber-supported catalysts. To the best of our understanding, no research has been done on synthesizing a NiMo/Graphene composite nanofibrous catalyst for the hydrocracking of heavy oils.

Our previous works studied hydro-cracking and hydro-treating of heavy hydrocarbons using Molybdenum-based catalysts prepared by impregnation techniques and supported on conventional metal oxide and carbon materials [36, 39-42]. In this work, NiMo/Graphene composite nanofibers and NiMo nanofibers supported on Graphene nanosheets were prepared via the electrospinning process, and their performances on the hydrocracking of n-hexadecane were compared with the Graphene-supported NiMo catalyst and also with the industrial γ -Alumina-supported NiMo catalysts synthesized by the wet impregnation method. The synthesized catalysts were analyzed for characterization using ICP, BET, TEM, FESEM, NH₃-TPD, and XRD techniques. The catalyst's performance was studied in terms of its activity, liquid product selectivity, and lifetime.

Experimental

Materials

Sigma-Aldrich (Germany) Company supplied graphite fine powder for the synthesis of graphene oxide. The commercial Ni-Mo/ γ -Al₂O₃ catalyst was sourced from the Bandar Abbas Oil Refinery (Iran). N-Hexadecane (used as the model feedstock component), nickel nitrate, and ammonium heptamolybdate were acquired from Merck. Polyvinylpyrrolidone (MW_{av}: 130 kDa) was provided by Sigma-Aldrich (Germany) Company to synthesize nanofibers.

Synthesis of Graphene Oxide Nanosheets

A modified Hummers process [6] created graphene oxide (GO) from graphite fine powders. Briefly, 2 g of graphite powder was dispersed into a 50 mL HNO₃: H₂SO₄ mixture under sonication in an ultrasonic bath (Elma S40H, Germany) for 30 min to remove impurities. Then, 1 g NaNO₃ and 6 g KMnO₄ were added to the solution, and sonication was continued for 30 minutes. To terminate the reaction, the suspension was further treated with H₂O₂ to remove the residual KMnO₄, followed by multiple washes with distilled water and subsequent drying in an oven at 80 °C for 8 hours.

Synthesis of GO-Supported NiMo Nanocatalysts

The NiMo/GO catalyst was synthesized via the impregnation method using (NH₄)₂MoS₄ and Ni(NO₃)₂ as the precursor salts. First, the predetermined amounts of Mo and Ni salts were dispersed in ethanol under sonication for 30 min. Then, the support particles were dispersed into the suspension under sonication for a further 120 min. Then, the synthesized sample was centrifuged and dried in an oven at 80 °C for 12 h. After the impregnation process, the catalyst was calcined at 450°C for 4 hours in an electrically heated quartz tube under a continuous N₂ flow of 50 mL min⁻¹. The composition of the synthesized catalyst is presented in Table 1.

Synthesis of NiMo Nanofibers Over the GO Support

The NiMo nanofibers were prepared via the electrospinning method, as described by Anis et al. [2]. Briefly, 10 wt.% PVP solution was prepared by dissolving 1 g PVP in ethanol for two h. Then, the prepared NiMo salts suspension (PVP/salts v:v 1:1) was added into the PVP solution under stirring for a further 12 h to obtain a homogeneous solution of PVP/salts. The applied voltage, tip-collector distance, flow rate, and collector speed were 22 kV, 12 cm, 0.5 mL/h, and 1000 rpm, respectively, for the fabrication of PVP/salts nanofibers. The electrospun fibers were calcined at 550 °C at a rate of 2 °C/min and kept there for two hours to remove the polymeric phase and break down the metal precursors at the same time. The synthesized fibers were dispersed into the GO suspension under stirring for four hours. Then, the synthesized sample was centrifuged and dried in an oven at 80 °C for 12 h. The synthesized catalyst's composition is shown in Table 1.

Synthesis of NiMo/GO Composite Nanofibrous Catalyst

The NiMo/GO nanofibrous catalyst was prepared via the electrospinning process in the presence of PVP. To prevent the agglomeration of nanosheets, the prepared GO/salts suspension was added drop-wise into the PVP solution, and sonication was continued for an additional three hours. Then, the PVP/GO/salts solution was transferred into the syringe with a needle gauge of 19 for the electrospinning process. The applied voltage, tip-collector distance, flow rate, and collector speed were constant at 22 kV, 12 cm, 0.5 mL/h, and 1000 rpm, respectively. The composition of the synthesized catalyst is presented in Table 1.

Catalyst Characterization

The Varian VISTA-MPX inductively coupled plasma-optical emission spectrometry (ICP-OES) equipment was used to assess the concentration of Ni and Mo metals on the catalysts. BET surface area, pore volume, and pore diameter of synthesized catalysts were measured using N₂ physisorption at 77 K in the ASAP-2010 Micromeritics system. The X-ray diffraction (XRD) analysis was performed utilizing a Philips PW1840 diffractometer equipped with monochromatized Cu/K α radiation. The measurements were carried out over an angular range



of 10–80° under a scanning speed of 0.03° (2 θ) s⁻¹. The half-width of a selected peak was entered into the Debye-Scherrer equation to get the crystallite diameter. The morphological characteristics of synthesized catalysts were examined using a field emission electron microscope (FESEM, Hitachi S-4160) and transmission electron microscope (TEM) (Philips). Image-ProPlus software from Media Cybernetics was used to measure the particle size distribution. The particle size distribution was created by measuring the particle sizes of at least 20 randomly chosen segments. The acidity of the synthesized catalysts was evaluated using temperature-programmed desorption of ammonia (NH₃-TPD) on a chemisorption physisorption analyzer (ChemBET Pulsar TPR/TPD, Quantachrome). 200 mg of the catalyst sample was pretreated at 500 °C for 3 hours. After the temperature was reduced to 50 °C, ammonia adsorption was conducted for 40 minutes. Any excess ammonia was then purged using helium at 50 °C for 2 hours. Finally, NH₃-TPD analysis was performed by heating the samples from 50 to 550 °C at 10 °C.min⁻¹, with a helium flow rate of 15 mL min⁻¹.

The coke/carbon deposits on the spent catalysts were measured by a common combustion method in a carbon analyzer, multi EA 2000, using a high-grade NDIR detector (Analytik Jena AG).

Reaction Testing and Analysis

The hydrocracking of n-hexadecane was carried out in a stainless steel fixed-bed tubular reactor, as illustrated in Fig. 1. Each experiment involved loading 2 grams of catalyst into the reactor, followed by reduction using hydrogen gas at a pressure of 30 bar and a space velocity of 600 h⁻¹. The temperature was gradually increased from ambient to 453 K at a heating rate of 0.5 K min⁻¹ and then maintained at this level for 1 hour. The catalysts were then subjected to a sulfidation process using a stream of 1 wt.% dimethyl disulfide in hexane, operating at a liquid hourly space velocity (LHSV) of 2 h⁻¹, a hydrogen pressure of 30 bar, and a hydrogen-to-oil volumetric ratio (H₂/Oil) of 80 nl/L to facilitate the formation of Ni-Mo-S active phases. The catalyst samples were subsequently heated from 453 K to 533 K at a rate of 0.5 K/min, followed by further heating from 533 K to 583 K at a rate of 2 K/min. The hydrocracking of n-hexadecane was then carried out at this temperature for 120 hours, during which the catalytic performance was evaluated. The reaction conditions included a temperature of 583 K, a H₂/n-hexadecane ratio of 175 nl/L, a pressure of 45 bar, and an LHSV of 1.4 h⁻¹.

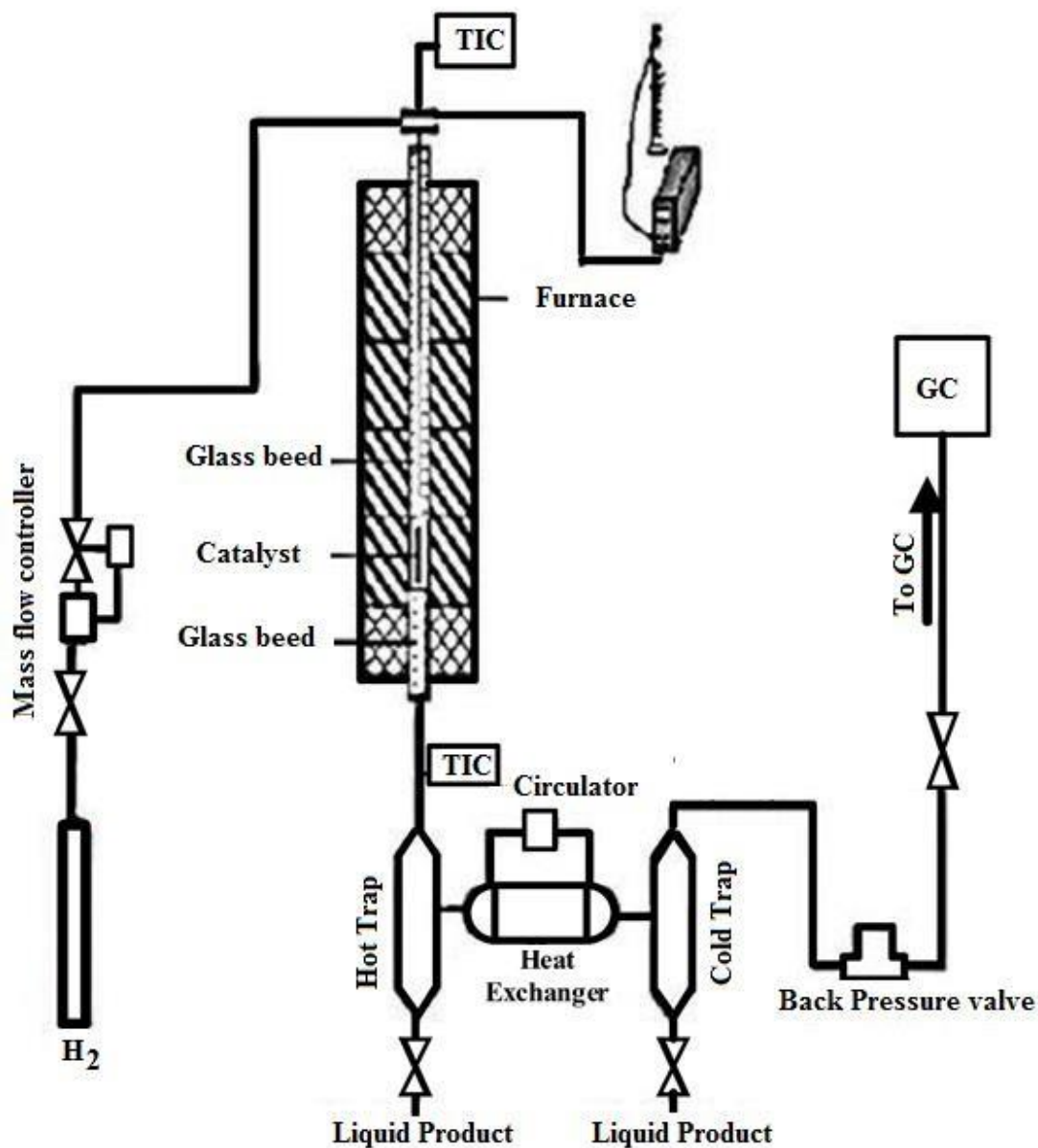


Fig. 1. The schematic of the experimental setup

The liquid products were collected every 12 h and analyzed using gas chromatography (Agilent 7890A), mass spectrometer (5975C VL MSD with triple-axis detector) equipped with a capillary column (Rtx 5 MS, HT-30 m long, 25 μ m film thickness). The percentage conversion of n-hexadecane and hydrocracking products yield was calculated as follows:

$$\text{Conversion-}C_{16} (\%) = \left(1 - \frac{(n-C_{16})_{out}}{(n-C_{16})_{in}}\right) \times 100 \quad (1)$$

$$\text{Yield} (\%) = \left(\frac{\text{Content of hydrocracking product formed}}{(n-C_{16})_{in}}\right) \times 100 \quad (2)$$

Result and Discussion

Characterization of Synthesized Catalysts

The physicochemical properties of the synthesized and industrial catalyst are presented in [Table 1](#). The Ni/(Ni+Mo) ratios are about ~0.3 for all the catalysts (ICP results). [Table 1](#) shows that nanofibrous catalysts' BET surface area and pore volume were higher than those of NiMo nanoparticles coated graphene nanosheets. The low surface area and pore volume in the case of NiMo/GNS catalysts may be attributed to the greater agglomeration of NiMo particles and pore blockage compared with nanofibrous catalysts. The fibrous structure of NiMo fibers/GNS and NiMo/GNS fibers catalysts can improve the mass transfer properties between the acidic and the metal sites, which facilitates the diffusion of reactants and promises the high activity of nanofibrous catalysts for the hydrocracking process. The surface area and pore volume are noticeably lower in the case of the industrial alumina-supported catalyst.

Table 1. Textural properties and chemical composition of synthesized catalysts

Catalyst/ support	Abbreviation	Ni (wt.%)	Mo (wt.%)	S _{BET} (m ² /g)	V _{total} (Cm ³ /g)	d _{avr} (nm)
NiMo/ Al ₂ O ₃	NMA	3.7	9.2	215	0.356	9.8
NiMo/GNS	NMG	3.5	8.8	542	0.565	2.15
NiMo fibers/GNS	NMFG	3.6	8.9	652	0.765	1.15
NiMo/GNS fibers	NMGF	3.7	9.1	824	0.925	0.89

The XRD patterns of Graphene, NMG, NMFG, and NMGF catalysts are illustrated in [Fig. 2](#). The main diffraction peaks observed at $2\theta = 23.3$ and 27.1° could be attributed to the (1 1 0) and (0 2 1) planes of MoO₃ orthorhombic phase in the NMFG and NMGF catalysts. The observed weak peak at $2\theta = 37.3^\circ$ was due to the (4 0 0) plane of the NiMoO₄ monoclinic phase. The XRD analysis indicated the presence of MoO₃ as a major phase compared with NiO as a minor phase in the NMFG catalyst. The weak diffraction peak for NiO was detected at $2\theta = 43.4^\circ$. A prominent reflection peak at $2\theta = 26^\circ$ was assigned to graphitic carbon. Furthermore, the XRD diffraction patterns of the catalysts showed more crystallite reflections of Mo or Ni metal oxides for nanofibrous catalysts compared with the NMG, which may be attributed to the uniform dispersion of fibers on the Graphene matrix compared with NiMo particles.

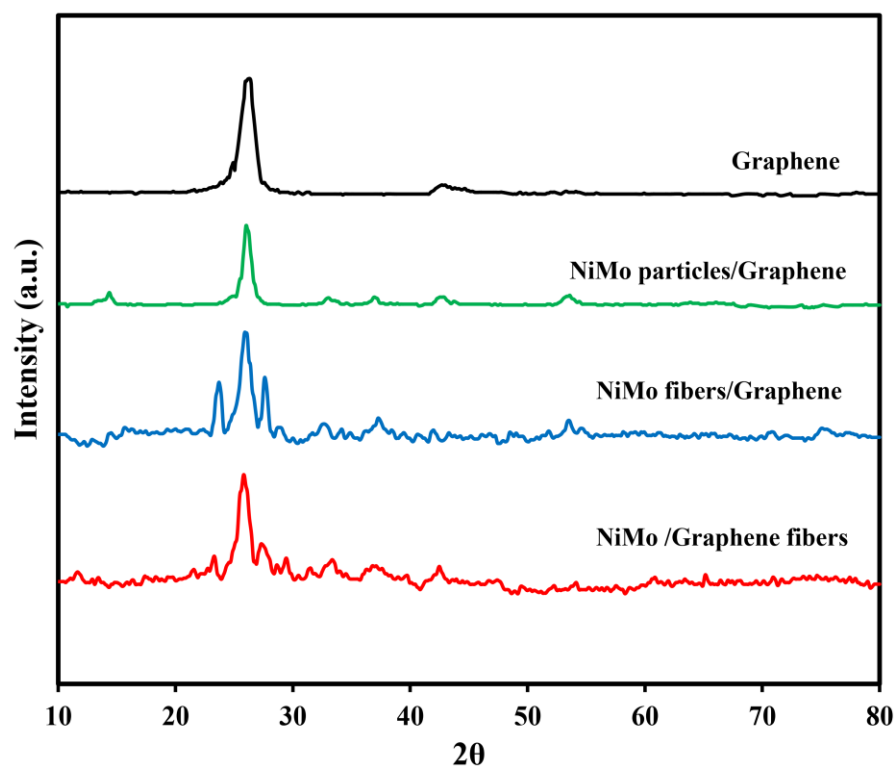


Fig. 2. XRD patterns of Graphene, NMG, NMFG and NMGF catalysts

The surface morphologies of the NMG, NMFG, and NMGF and particle/fiber size distribution are illustrated in Fig. 3. The TEM image of NMG revealed a high dispersion of NiMo particles across the surface of the NMG catalyst, as shown in Fig. 3a. The dark spots could be attributed to the attachment of the NiMo particles to the Graphene surface support. As shown, graphene channels restrict the growth of particles. Also, Fig. 3a illustrates the size distribution of the metal particles, which is calculated using data from four TEM images (one of which is presented in this manuscript) and the population of about 100 metal particles of the catalysts. This figure and the TEM images depict a narrow nanoparticle size distribution on graphene. The size distribution of the particles ranged from 2-7 nm.

As shown in Fig. 3b, the smooth NiMo fibers without beads, ranging from 20 to 100 nm with an average diameter of 67 nm, were produced on the graphene nanosheet surface. Uniform fibers with higher fiber diameters were obtained for NiMo/GNS fibers (Fig. 3c). The fiber diameter distribution ranged from 50-250 nm with an average diameter of 160 nm.

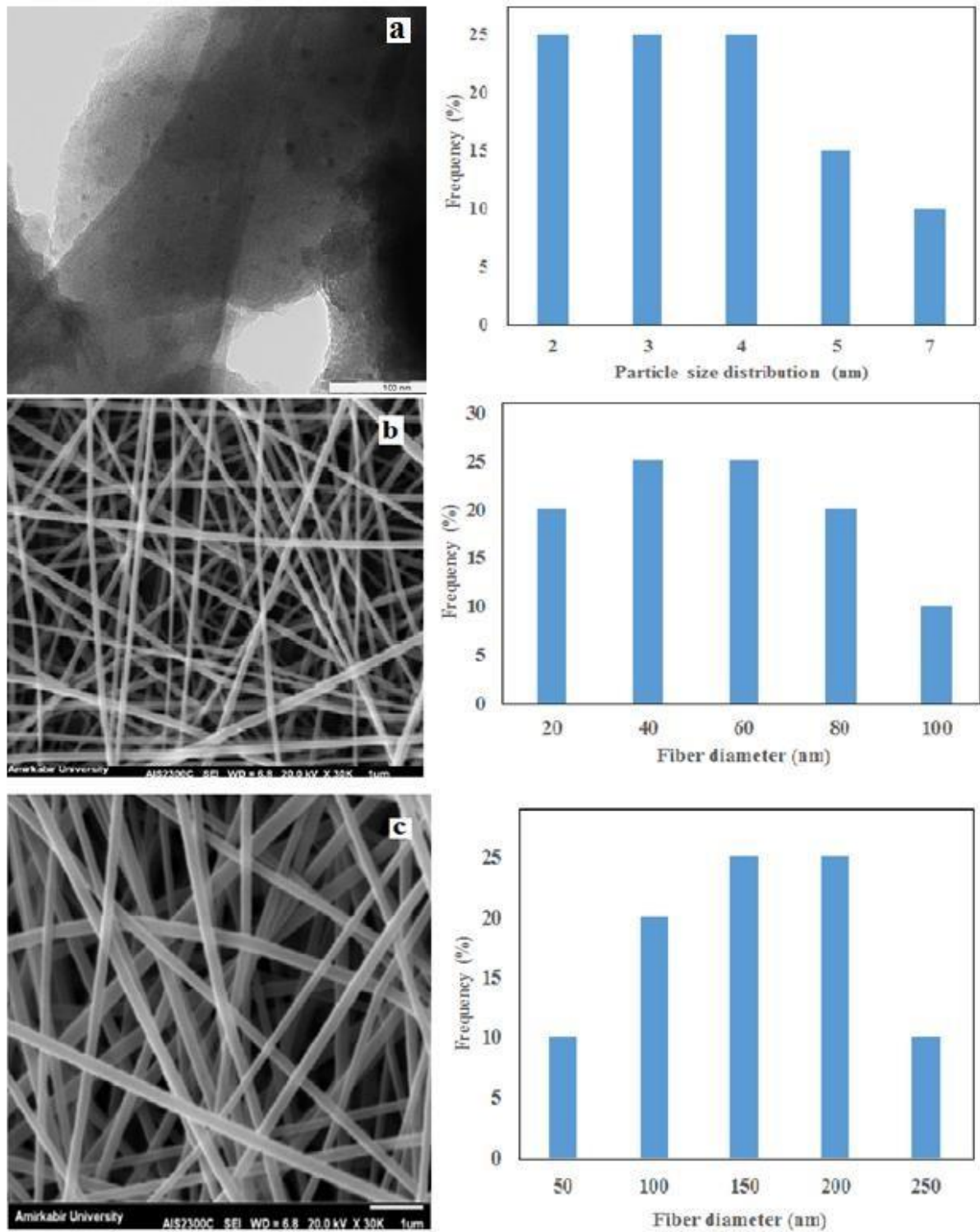


Fig. 3. (a) TEM image and particle size distribution of NMG, (b), (c) FESSEM images and particle size distributions of NMFG and NMGF catalysts

The NH₃-TPD profiles of synthesized catalysts are depicted in Fig. 4. The acid site distributions of the catalysts are also displayed in Table 2. The synthesized catalysts showed different distributions of acidic sites (weak, medium, and strong acidic sites were considered for temperatures lower than 200 °C, between 200 and 400 °C, and higher than 400 °C). The NMFG and NMGF nanofibrous catalysts with a total acidity of 521.4 and 563.8 μmolg^{-1} had enough acidic sites for n-hexadecane cracking, which could be attributed to the high surface area and large pore volume of fibrous catalysts compared with the NMG catalyst with a total acidity of 186.6 μmolg^{-1} . The reduced diffusion and adsorption of NH₃ molecules from the NMG catalyst's pores may cause the catalyst's decreased acidity. The order of the number of strong acidic sites is NMGF>NMFG>NMG.

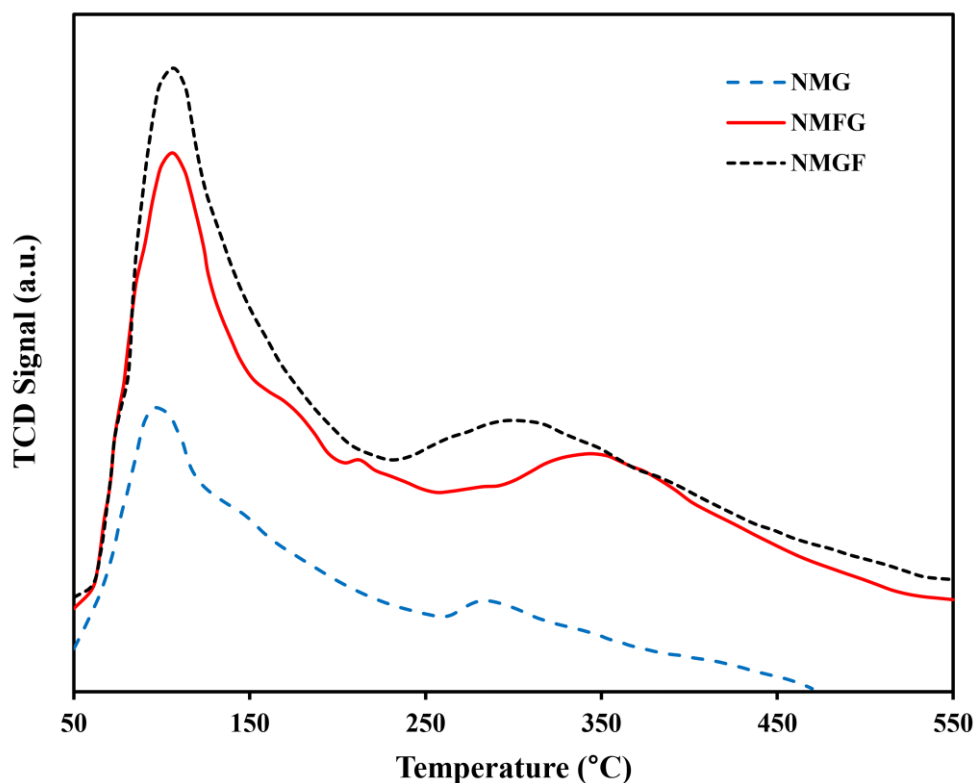


Fig. 4. NH₃-TPD profiles of synthesized NMG, NMFG, and NMGF

Table 2. Acid site distribution in the synthesized catalysts

Catalyst	NH ₃ content ($\mu\text{mol/g}$ catalyst)			Total acid site
	Weak acid site	Medium acid site	Strong acid site	
NMG	76.9	76.4	33.3	186.6
NMFG	216.1	189.9	115.4	521.4
NMGF	240.1	200.4	123.3	563.8

Performance of Synthesized Catalysts on C₁₆ Hydrocracking

The total conversion and product selectivity for commercial NiMo/ γ -Al₂O₃ catalysts and synthesized NMG, NMFG, and NMGF catalysts have been investigated for 120 h. The results for the first 12 h synthesis are illustrated in Table 3. Only 63% conversion was observed for the commercial NiMo/ γ -Al₂O₃ catalyst. Meanwhile, 85.1, 99.2, and 99.5% total conversion of n-C₁₆ were achieved using NMG, NMFG, and NMGF catalysts, respectively. The synthesized



nanofibrous catalysts showed a higher conversion of n-C₁₆ than the NMG catalyst. This behavior may be attributed to the uniform dispersion of fibers compared with the dispersion of nanoparticles on the Graphene nanosheets, with some agglomeration of NiMo particles as described by TEM and FESEM images. The hydrocracking of n-C₁₆ consists of the hydrogenation at metal sites, followed by cracking at acidic sites of the support, where it occurs. The better balance between the metal sites of NiMo and acid sites of graphene supports led to high cracking and hydrogenation activity of the synthesized catalysts. The strong acid sites of supports of NMG, NMFG, and NMGF catalysts resulted in the high conversion of synthesized catalysts for n-C₁₆ hydrocracking. Furthermore, increasing the surface area enhanced the accessibility of feed molecules to the catalyst's active sites.

Table 3. Percentage conversion and product yield in the presence of different catalysts

Catalyst	Conversion (%)	Gaseous products (%)	Liquid products (%)
NMA	63	4.3	95.7
NMG	85.1	5.4	94.6
NMFG	99.2	7.9	92.1
NMGF	99.5	8.4	91.6

The product yield during the first 12 h of n-C₁₆ hydrocracking is also presented in [Table 3](#). Comparing the results of the synthesized NMG, NMFG, and NMGF catalysts with those obtained from the industrial catalyst demonstrates that the quantity of gaseous products rises. In contrast, the quantity of liquid products reduces. The support porosity, the number and strength of acid sites, and the distance between the two catalytic functions can affect the catalyst's selectivity in the hydrocracking process. The cracking is significantly influenced by the strength of the individual type of sites rather than the total concentration. The cracking mainly takes place on Brønsted acid sites. The cracking ability of catalysts follows the same trend as the Brønsted acidity. However, in a bifunctional catalyst, the balance between its two catalytic functions is crucial in determining its overall performance. Enhancing the hydrogenation capability (which takes place on the metal sites of NiMo) can lead to a notable improvement in selectivity toward light products. This occurs by accelerating the desorption rate of carbocations, thereby minimizing the extent of secondary cracking on NMG, NMFG, and NMGF catalysts. The distributions of liquid hydrocarbon products from hydrocracking of n-hexadecane using synthesized NMG, NMFG, NMGF and NMA catalysts are presented in [Fig. 5](#). Also, the distribution of the C₆ isomers (n-hexane (nC₆), 2-methylpentane (2MP), 3-methylpentane (3MP), 2,3-dimethylbutane (23DMB), and 2,2-dimethylbutane (22DMB)) for the reaction with NMGF catalyst is shown on the left corner of this figure. Due to the reactor's high partial pressure of hydrogen, most of the C₆ isomers are saturated hydrocarbons. As indicated, the main liquid hydrocarbon component produced during the hydrocracking of n-C₁₆ using NMG, NMFG, and NMGF catalysts was C₅-C₁₂ alkanes. The appropriate balance between nanofibrous catalysts' textural and acidic properties resulted in the selective hydrocracking of n-C₁₆.

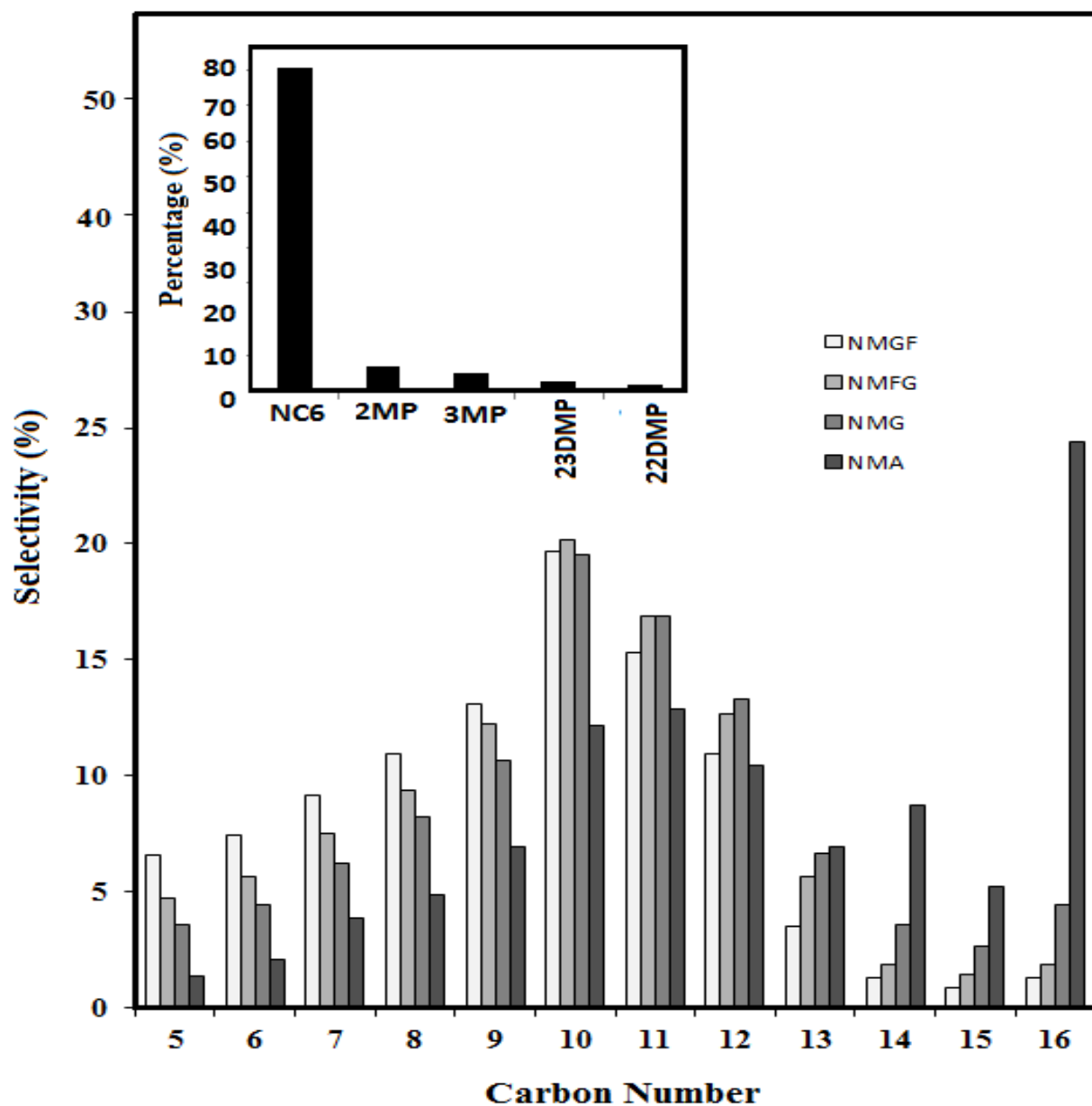


Fig. 5. Liquid hydrocarbon products distribution from hydrocracking of n-hexadecane

Fig. 6 shows the percentage conversion variations with the reaction duration for different catalysts. This figure shows that the catalysts displayed different stability patterns within 120 h of continuous n-C16 hydrocracking. In the case of commercial NMA catalyst, 120 h of continuous reaction decreased the percentage conversion from 63 to 56.6 (6.4% decrease). The conversion severely decreased on the first day and then leveled off. The decreases for NMG, NMFG, and NMGF catalysts were 5.5, 2.3, and 1.9%, respectively. The commercial and NMG

catalysts were deactivated significantly over time, and almost complete conversion of n-C₁₆ took place with the nanofibrous catalysts.

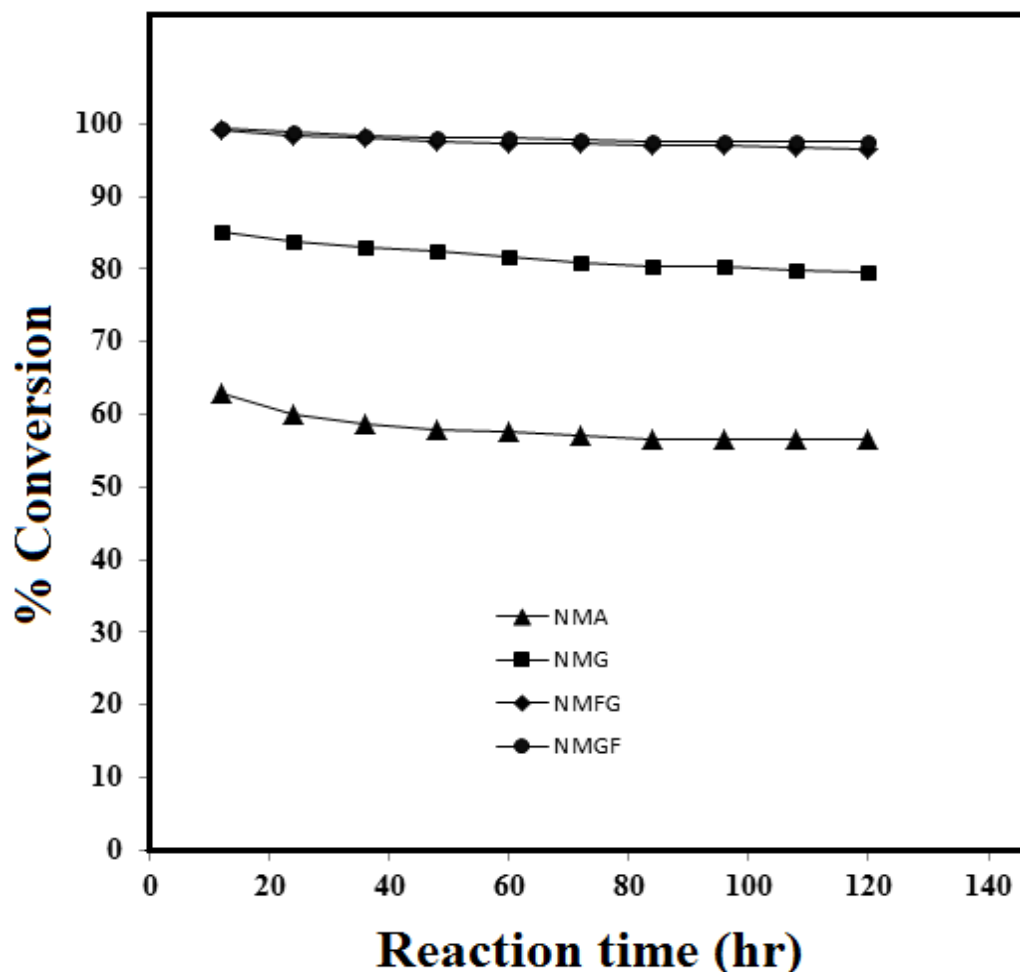


Fig. 6. Variations of %Conversion with time for different catalysts

The more coke formation during hydrocracking of n-C₁₆ could be responsible for the deactivation of commercial NMA and NMG catalysts. Table 4 shows the percentage of coke deposits during n-C₁₆ hydrocracking. The coke formation on the catalyst can result in the catalyst deactivation via the coke deposits in the catalyst pores and catalyst surface, followed by the blocking of pores and surface area loss. On the other hand, the reduction in the activity of the catalyst occurs through the non-volatile carbonaceous deposits that incorporate into the catalyst pores or adsorb on the catalyst surface. The catalyst properties, such as acidity, surface area, and pore size distribution, can affect the coke deposition. The minimum coke deposition was obtained for the NMGF nanofibrous catalyst. The faster kinetics of the hydrocracking process using nanofibrous catalysts may lead to fewer coke deposits. Furthermore, the higher surface area of the catalyst and the larger intra-fiber distance (large pore volume) could be responsible for the lower coke formation on the catalyst. The low coke formation can reduce the loss of liquid products and increase the production of valuable products via the hydrocracking of heavy oils.

Table 4. Percentage of coke deposition during n-C₁₆ hydrocracking using different catalysts

Catalyst/ support	Coke (%)
NiMo/ Al ₂ O ₃	1.85
NiMo/GNS	0.45
NiMo fibers/GNS	0.25
NiMo/GNS fibers	0.22

Due to its higher activity and productivity, using the catalyst prepared in this research in the existing industrial reactors will increase the production of lighter products, especially middle distillation products. Also, using this catalyst in the design of new hydrocracking plants will reduce the size of the reactor. Both of the above cases will improve the economic aspects of the hydrocracking plants. In addition, increasing the lifetime of the catalyst and reducing the production of coke on the catalyst will increase the exploitation period and continuous operation time on the reactor stream, and this issue will also have positive effects on the economic factors of the process.

Conclusion

Nanofibrous catalysts were successfully developed for the hydrocracking of heavy oils in a fixed-bed reactor. The characteristics of synthesized nanofibrous catalysts indicated a high surface area, large pore volume, and more strong acidic sites. The synthesized fibrous catalysts exhibited more catalyst activity for hydrocracking than NiMo nanoparticles coated graphene and a commercial NiMo/Al₂O₃ catalyst. The lighter hydrocarbons were achieved in hydrocracking using nanofibrous catalysts. Nanofibrous catalysts resulted in a more stable catalyst compared with their counterparts.

Abbreviation

NMGF	Nickel Molybdenum/Graphene composite nanofibers
NMFG	Nickel Molybdenum nanofibers supported on Graphene nanosheets
NMA	Nickel Molybdenum /Al ₂ O ₃
NMG	Nickel Molybdenum/Graphene
ICP	Inductively Coupled Plasma
FESEM	Field Emission Scanning Electron Microscope
TEM	Transmission Electron Microscopy
XRD	X-ray Diffraction
FBR	Fixed-Bed Reactors
GNS	Graphene nanosheets
NH ₃ -TPD	Temperature-Programmed Desorption of Ammonia

References

- [1] Anis S F, Singaravel G and Hashaikeh R (2017) Electropsun Ni-W/zeolite composite fibers for n- heptane hydrocracking and hydroisomerization. *Materials Chemistry and Physics*, 200146-154. <https://doi.org/https://doi.org/10.1016/j.matchemphys.2017.07.081>.
- [2] Anis S F, Singaravel G and Hashaikeh R (2018) Hierarchical nano zeolite-Y hydrocracking composite fibers with highly efficient hydrocracking capability. *RSC advances*, 830: 16703-16715. <https://doi.org/DOI: 10.1039/C8RA02662A>.
- [3] Bouchy C, Hastoy G, Guillon E and Martens J (2009) Fischer-Tropsch waxes upgrading via hydrocracking and selective hydroisomerization. *Oil & Gas Science and Technology- Revue de l'IFP*, 641: 91-112. <https://doi.org/DOI: 10.2516/ogst/2008047>.
- [4] Chang J, Tsubaki N and Fujimoto K (2001) Elemental sulfur as an effective promoter for the catalytic hydrocracking of Arabian vacuum residue. *Fuel*, 8011: 1639-1643. [https://doi.org/https://doi.org/10.1016/S0016-2361\(01\)00035-7](https://doi.org/https://doi.org/10.1016/S0016-2361(01)00035-7).
- [5] Kayukova G, Mikhailova A, Kosachev I, Feoktistov D A and Vakhin A (2018) Conversion of heavy oil with different chemical compositions under catalytic aquathermolysis with an amphiphilic Fe-Co-Cu catalyst and kaolin. *Energy & fuels*, 326: 6488-6497. <https://doi.org/https://doi.org/10.1021/acs.energyfuels.8b00347>.
- [6] Chuan L, Bin S, Min C, SHANG H-y and QUE G-h (2007) Application of Co-Mo/CNT catalyst in hydro-cracking of Gudao vacuum residue. *Journal of Fuel Chemistry and Technology*, 354: 407-411. [https://doi.org/https://doi.org/10.1016/S1872-5813\(07\)60026-7](https://doi.org/https://doi.org/10.1016/S1872-5813(07)60026-7).
- [7] Hummers Jr W S and Offeman R E (1958) Preparation of graphitic oxide. *Journal of the american chemical society*, 806: 1339-1339. <https://doi.org/https://doi.org/10.1021/ja01539a017>.
- [8] Kalbasi R J, Massah A R and Barkhordari Z (2010) An efficient and green approach for the esterification of aromatic acids with various alcohols over H₃PO₄/TiO₂-ZrO₂. *Bulletin of the Korean Chemical Society*, 318: 2361-2367. <https://doi.org/https://doi.org/10.5012/bkcs.2010.31.8.2361>.
- [9] Kaminski T, Anis S F, Husein M M and Hashaikeh R (2018) Hydrocracking of athabasca VR using NiO-WO₃ zeolite-Based catalysts. *Energy & Fuels*, 322: 2224-2233. <https://doi.org/https://doi.org/10.1021/acs.energyfuels.7b03754>.
- [10] Kham-or P, Suwannasom P and Ruangviriyachai C (2016) Effect of agglomerated NiMo HZSM-5 catalyst for the hydrocracking reaction of *Jatropha curcas* oil. *Energy Sources, Part A: Recovery, Utilization, and Environmental Effects*, 3824: 3694-3701. <https://doi.org/https://doi.org/10.1080/15567036.2016.1166165>.
- [11] Kim H, Nguyen-Huy C and Shin E W (2014) Macroporous NiMo/alumina catalyst for the hydrocracking of vacuum residue. *Reaction Kinetics, Mechanisms and Catalysis*, 1132: 431-443. <https://doi.org/https://doi.org/10.1007/s11144-014-0764-5>.
- [12] Kim S K, Yoon D, Lee S-C and Kim J (2015) Mo₂C/graphene nanocomposite as a hydrodeoxygenation catalyst for producing diesel range hydrocarbons. *Acs Catalysis*, 56: 3292- 3303. <https://doi.org/https://doi.org/10.1021/acscatal.5b00335>.
- [13] Kim Y-S, Yun G-N and Lee Y-K (2014) Novel Ni₂P/zeolite catalysts for naphthalene hydrocracking to BTX. *Catalysis Communications*, 45133-138. <https://doi.org/https://doi.org/10.1016/j.catcom.2013.11.010>.
- [14] Lee J, Choi Y, Shin J and Lee J K (2016) Selective hydrocracking of tetralin for light aromatic hydrocarbons. *Catalysis Today*, 265144-153. <https://doi.org/https://doi.org/10.1016/j.cattod.2015.09.046>.
- [15] Liang J, Liang Z, Zou R and Zhao Y (2017) Heterogeneous catalysis in zeolites, mesoporous silica, and metal-organic frameworks. *Advanced Materials*, 2930: 1701139. <https://doi.org/10.1002/adma.201701139>.

- [16] Liu J, He J, Wang L, Li R, Chen P, Rao X, Deng L, Rong L and Lei J (2016) NiO-PTA supported on ZIF-8 as a highly effective catalyst for hydrocracking of Jatropha oil. *Scientific reports*, 61: 1-11. <https://doi.org/https://doi.org/10.1038/srep23667>.
- [17] Manrique C, Guzmán A, Pérez-Pariente J, Márquez-Álvarez C and Echavarría A (2016) Vacuum gas- oil hydrocracking performance of Beta zeolite obtained by hydrothermal synthesis using carbon nanotubes as mesoporous template. *Fuel*, 182236-247. <https://doi.org/https://doi.org/10.1016/j.fuel.2016.05.097>.
- [18] Morel F, Kressmann S, Harlé V and Kasztelan S (1997) Processes and catalysts for hydrocracking of heavy oil and residues. In *Studies in surface science and catalysis Vol. 106*, pp. 1-16. Elsevier. [https://doi.org/https://doi.org/10.1016/S0167-2991\(97\)80003-1](https://doi.org/https://doi.org/10.1016/S0167-2991(97)80003-1).
- [19] Okunev A, Parkhomchuk E V e, Lysikov A I, Parunin P D, Semeykina V and Parmon V N (2015) Catalytic hydroprocessing of heavy oil feedstocks. *Russian chemical reviews*, 849: 981. <https://doi.org/DOI 10.1070/RCR4486>.
- [20] Park K-C and Ihm S-K (2000) Comparison of Pt/zeolite catalysts for n-hexadecane hydroisomerization. *Applied Catalysis A: General*, 2032: 201-209. [https://doi.org/https://doi.org/10.1016/S0926-860X\(00\)00490-7](https://doi.org/https://doi.org/10.1016/S0926-860X(00)00490-7).
- [21] Purón H, Pinilla J, Suelves I and Millan M (2015) Acid treated carbon nanofibers as catalytic support for heavy oil hydroprocessing. *Catalysis Today*, 24979-85. <https://doi.org/https://doi.org/10.1016/j.cattod.2014.09.021>.
- [22] Rad M R, Rashidi A, Vafajoo L and Rashtchi M (2014) Preparation of Co–Mo supported multi-wall carbon nanotube for hydrocracking of extra heavy oil. *Journal of Industrial and Engineering Chemistry*, 206: 4298-4303. <https://doi.org/https://doi.org/10.1016/j.jiec.2014.01.036>.
- [23] Rana M S, Sámano V, Ancheyta J and Diaz J (2007) A review of recent advances on process technologies for upgrading of heavy oils and residua. *Fuel*, 869: 1216-1231. <https://doi.org/https://doi.org/10.1016/j.fuel.2006.08.004>.
- [24] Sahu R, Song B J, Im J S, Jeon Y-P and Lee C W (2015) A review of recent advances in catalytic hydrocracking of heavy residues. *Journal of Industrial and Engineering Chemistry*, 2712-24. <https://doi.org/https://doi.org/10.1016/j.jiec.2015.01.011>.
- [25] Subsadsana M, Sansuk S and Ruangviriyachai C (2018) Enhanced liquid biofuel production from crude palm oil over synthesized NiMoW-ZSM-5/MCM-41 catalyst. *Energy Sources, Part A: Recovery, Utilization, and Environmental Effects*, 402: 237-243. <https://doi.org/https://doi.org/10.1080/15567036.2017.1411992>.
- [26] Sun C, Zhan T, Pfeifer P and Dittmeyer R (2017) Influence of Fischer-Tropsch synthesis (FTS) and hydrocracking (HC) conditions on the product distribution of an integrated FTS-HC process. *Chemical Engineering Journal*, 310272-281. <https://doi.org/https://doi.org/10.1016/j.cej.2016.10.118>.
- [27] Taylor R J and Petty R H (1994) Selective hydroisomerization of long chain normal paraffins. *Applied Catalysis A: General*, 1191: 121-138. [https://doi.org/https://doi.org/10.1016/0926-860X\(94\)85029-1](https://doi.org/https://doi.org/10.1016/0926-860X(94)85029-1).
- [28] Trépanier M, Tavasoli A, Dalai A K and Abatzoglou N (2009) Co, Ru and K loadings effects on the activity and selectivity of carbon nanotubes supported cobalt catalyst in Fischer–Tropsch synthesis. *Applied Catalysis A: General*, 3532: 193-202. <https://doi.org/https://doi.org/10.1016/j.apcata.2008.10.061>.
- [29] Trépanier M, Tavasoli A, Dalai A K and Abatzoglou N (2009) Fischer–Tropsch synthesis over carbon nanotubes supported cobalt catalysts in a fixed bed reactor: Influence of acid treatment. *Fuel Processing Technology*, 903: 367-374. <https://doi.org/https://doi.org/10.1016/j.fuproc.2008.10.012>.
- [30] Upare D P, Park S, Kim M, Jeon Y-P, Kim J, Lee D, Lee J, Chang H, Choi S and Choi W (2017) Selective hydrocracking of pyrolysis fuel oil into benzene, toluene and xylene over CoMo/beta zeolite catalyst. *Journal of Industrial and Engineering Chemistry*, 46356-363. <https://doi.org/https://doi.org/10.1016/j.jiec.2016.11.004>.
- [31] Wang X, Xu W, Liu N, Yu Z, Li Y and Qiu J (2015) Synthesis of metallic Ni-Co/graphene catalysts with enhanced hydrodesulfurization activity via a low-temperature plasma

- approach. *Catalysis Today*, 256203-208. <https://doi.org/https://doi.org/10.1016/j.cattod.2015.04.026>.
- [32] Weiss W, Guibard I and Dastillong R (2018) Process for hydroconverting oil feeds in fixed beds to produce low sulphur fuels. In: Google Patents.
- [33] Xing T, Alvarez-Majmutov A and Chen J (2019) Bitumen partial upgrading by mild hydroprocessing in a fixed-bed reactor. *Fuel*, 235696-702. <https://doi.org/https://doi.org/10.1016/j.fuel.2018.08.058>.
- [34] Yang L, Wang X, Liu Y, Yu Z, Li R and Qiu J (2017) Layer-dependent catalysis of MoS₂/graphene nanoribbon composites for efficient hydrodesulfurization. *Catalysis Science & Technology*, 73: 693-702. <https://doi.org/DOIhttps://doi.org/10.1039/C6CY02074G>.
- [35] Yuan L, Wang X, Zhao K, Pan H, Li Q, Yang J and Zhang Z (2017) Effect of reaction temperature and hydrogen donor on the NiO@ graphene-catalyzed viscosity reduction of extra heavy crude oil. *Petroleum Science and Technology*, 352: 196-200. <https://doi.org/https://doi.org/10.1080/10916466.2016.1241805>.
- [36] Yusefabad E T, Tavasoli A and Zamani Y (2018) Effective catalyst to produce naphtha from vacuum gasoil hydrocracking and discrete lump modeling. *Petroleum & Coal*, 601. <https://doi.org/Corpus ID: 195890031>.
- [37] Bamdadi M, Bozorg A, Tavasoli A, Shateri S, Andache M (2019) Synthesis of Meso/Macroporous γ - Alumina via Aluminum Pellet with Controllable Porosity: Ammonium Bicarbonate Influences through Drying and Calcination Steps. *Chemistry Select* 4 (19), 5872-5879. <https://doi.org/10.1002/slct.201900523>.
- [38] Hashemi H, Behnejad H, Rosendahl, L Tavasoli A (2022) Tuning the porosity and physicochemical properties of SBA-15: RSM-assisted optimizing of traditional sol-gel process , *Chemical Papers* vol 76, 4541-4560. <https://doi.org/10.1007/s11696-022-02187-z>.
- [39] Salimi M, Tavasoli A, Rosendahl L (2020) Optimization of γ -alumina porosity via response surface methodology: the influence of engineering support on the performance of a residual oil hydrotreating catalyst, *Microporous and Mesoporous Materials* 299, 110124. <https://doi.org/10.1016/j.micromeso.2020.110124>.
- [40] B. Liu, H. Lv, X. Cui, G. Sun, X. Zhang, B. Dong, Y. Li, Y. Pan, Y. Chai, C. Liu, Preparation of presulfided oil-soluble NiMo catalyst for slurry bed hydrocracking of vacuum residue, *Chemical Engineering Journal*, 498 (15), 2024. <https://doi.org/10.1016/j.cej.2024.155166>.
- [41] D. Dhaneswara, J. Fatriansyah, T. Sudiro, S. Harjanto, M. S. Mastuli, A. Federico, R. Ulfiati, Synthesis and optimization of Ni/Mo-impregnated kaolin-based ZSM-5 as a catalytic hydrocracking catalyst for heavy petroleum distillates, *Sustainable Energy & Fuels*, 12, 2024. <https://doi.org/10.1039/d3se01573d>.
- [42] K.K. Ferreira, C. Di Stasi, A. Ayala-Cortés, L.S. Ribeiro, J.L. Pinilla, I. Suelves, M.F.R. Pereira, Hydroprocessing of waste cooking oil to produce liquid fuels over Ni-Mo and Co-Mo supported on carbon nanotubes, *Biomass and Bioenergy*, 91, 2024. <https://doi.org/10.1016/j.biombioe.2024.107480>.

How to cite: Zanjanejad B, Norozi A, Babatabar M, Tavasoli A. Synthesis and Application of Electropun Nickel-Molybdenum/Graphene Composite Nanofibers and Nickel-Molybdenum Nanofibers Supported on Graphene Nanosheets Catalysts for Hydrocracking of Heavy Hydrocarbons. Journal of Chemical and Petroleum Engineering 2025; 59(1): 141-157.